Fluid Dynamics and Co-located Conferences
June 24-27, 2013, San Diego, CA
43rd Fluid Dynamics Conference

Submitted to 43rd AIAA Fluid Dynamics Conference and Exhibit, 24-27 June 2013, San Diego, California

Multi-Objective Design Optimization of a Transonic Compressor Rotor Using an Adjoint Equation Method

Jiaqi Luo*
Peking University, Beijing 100871, China
Feng Liu†
University of California, Irvine, CA 92697-3975, United States

This paper presents the application of a viscous adjoint method to the multi-objective design optimization of a transonic compressor rotor blade row. The adjoint method requires about twice the computation effort of flow calculation to obtain the complete gradient information for each cost function, regardless of the number of design parameters. NASA Rotor 67 is redesigned to maximize the total pressure ratio and adiabatic efficiency. The multi-objective design optimization is decomposed into multiple single-objective design optimizations. Firstly a set of blades with different gains of total pressure ratio can be obtained through the design initialization maximizing total pressure ratio with the constraint of mass flow rate. The upper limit of total pressure ratio can be predicted to avoid stall in the design. Then a series of single-objective optimizations maximizing adiabatic efficiency for fixed total pressure ratio are performed starting from the blades determined in the initial step to obtain the Pareto front. The cost function is defined as the entropy production per unit mass flow rate combined with the constraints of mass flow rate and total pressure ratio. The results are presented in detail and the effects of blade profile modification on performance improvement and shock/tip-leakage interaction are examined.

Nomenclature

$\mathbf{A}_j$	Jacobian matrices, $\mathbf{A}_j = \partial \mathbf{f}_j / \partial \mathbf{w}$
$\mathbf{B}_s$	Source matrix, $\mathbf{B}_s = \partial \mathbf{S} / \partial \mathbf{w}$
$\mathbf{f},\ \mathbf{f}_v$	Inviscid and viscous fluxes
n_j	Unit normal vector in the computational domain
$p_0,\ \rho_0$	References of pressure and density
$\mathbf{R}$	Flow governing equation
$\mathbf{S}$	Source term
u_j	Absolute velocity components
$\hat{u}_j$	Grid velocity components
$\mathbf{w}$	Conservative flow variables, $\mathbf{w} = \{\rho, \rho u, \rho v, \rho w, \rho E\}^T$
β	Flow turning
Δs	Entropy, $\Delta s = c_v ln(p/p_0) - c_p ln(\rho/\rho_0)$
η	Adiabatic efficiency
Λ	Weight of penalty function
Ω	Rotation velocity
π	Total pressure ratio
Ψ	Adjoint variables, $\Psi = \{\psi_1, \psi_2, \psi_3, \psi_4, \psi_5\}^T$
σ	Ratio of mass flow rate, $\sigma = \dot{m}/\dot{m}_0$
θ	Total temperature ratio

*Post-doctoral Researcher, College of Engineering. jiaqil81@gmail.com
†Professor, Department of Mechanical and Aerospace Engineering, AIAA Fellow. fliu@uci.edu

I. Introduction

By using Computational Fluid Dynamics (CFD), many research papers on design optimization of compressor blades have been published in recent years.[1–4] Oyama et al.[1] performed design optimization of the NASA Rotor 67 to reduce entropy production by using an Evolutionary Algorithm and obtain approximately 2% efficiency gain. The maximal discrepancies of total pressure ratio and mass flow rate of their optimized blade were about 1% and 0.5%, respectively, compared with those of the reference blade. In order to minimize the weight and size of an aircraft engine, one strives to increase both the total pressure ratio and adiabatic efficiency of the compressor. Hence multi-objective design optimization has been proposed and studied to satisfy the higher level requirements. Benini[3] successfully performed multi-objective design optimization of the NASA Rotor 37 to maximize the total pressure ratio and compressor efficiency. Lian and Liou[4] redesigned the Rotor 67 blade by maximizing the total pressure ratio, while minimizing the compressor weight; and an approximately 1.8% total pressure ratio gain was achieved.

Evolutionary Algorithm has been widely used to both external and internal optimization due to its robustness and excellent compatibility in design optimization. However, thousands of flow calculations are necessary in each design cycle because numerous populations and individuals are required to support the global optimal by using this method. In contrast, optimization by using the adjoint method can significantly improve computational efficiency because it requires about only two flow calculations in each design cycle to determine the complete gradient information needed in the optimization, regardless of the number of design parameters.

The adjoint method, proposed by Jameson,[5,6] is one of the gradient-based optimization methods. Due to its high-efficiency and sufficient accuracy on gradient calculation, it has been used in the optimization of airfoils, wing, wing-body configurations. In recent years, this high-efficiency optimization method was introduced to the design optimizations of turbomachinery blades. Liu et al.[7,8] successfully applied this method to the optimization of cascade and turbine blade. Luo et al.[9–11] performed design optimization of turbine blades to reduce shock loss, profile loss and secondary flow loss through modifying blade profile, restaggering and endwall contouring by using a continuous adjoint method; subsequently, they successfully performed multi-point optimization of a transonic compressor rotor to improve the aerodynamic performance over the whole operating range.[12] Wang et al.[13,14] and Nadarajah et al.[15] presented the applications of the adjoint method to the design optimizations of multi-stages.

Compared with the non-gradient-based method, one of the drawbacks of multi-objective design optimization by using the gradient-based method is that the Pareto front cannot be obtained by only one design optimization process. Some research papers on the gradient-based multi-objective design optimization have been published .[16–19] A simple approach is the weighted-sum method,which converts the multi-objective optimization problem to a single-objective optimization problem with a single cost function consisting of a linear combination of multiple cost functions with appropriate weights. For a weighted cost function

$$I = \sum_{i=1}^{N} \lambda_i f_i(\mathbf{x}) \tag{1}$$

where I is the cost function; N is the number of objectives; λ_i satisfy $\sum_{i=1}^{N} \lambda_i = 1$ and $\lambda_i > 0$; $\mathbf{x}$ is the design space. The design converges at

$$\sum_{i=1}^{N} \lambda_i \nabla f_i(\mathbf{x}^*) = 0 \tag{2}$$

Eq. (2) means that the weighted gradient approaches zero at design convergence. $\mathbf{x}^*$ is one of the Pareto solutions. However, as pointed out by Shankaran and Barr[17] that this method is unable to capture the concave portions and disjoint Pareto fronts. Besides, this method cannot always guarantee sufficient design convergence because the improvement of some objectives brings with other defects not allowed in reality. For example, in the multi-objective optimization of total pressure ratio and adiabatic efficiency of a transonic compressor rotor, the total pressure ratio is not allowed to increase without limit because the rotor blade approaches stall as the total pressure ratio increases, even at the design point.

In the present study, a continuous adjoint method is introduced to the multi-objective design optimization of the transonic compressor rotor blade NASA Rotor 67 to maximize both the total pressure ratio and

adiabatic efficiency at the operating condition near peak efficiency with the constraint of mass flow rate. The increment of total pressure ratio is hard to be controlled with only constraint of mass flow rate. Increasing total pressure ratio induces (1) increased turning to a critical degree, after that the mass flow rate decreases away from the constraint; and (2) compressor stall triggers at a lower back pressure due to the stronger shock and the more intensive shock/tip-leakage interaction. The detrimental performance in the multi-objective design optimization brings difficulties on obtaining the converged optimal aerodynamic shape. Hereby the multi-objective design optimization studied in the present paper is decomposed into a series of single-objective design optimizations. The reference blade is firstly optimized to maximize the total pressure ratio and predict an approximate upper limit at the design point. Then the blades with different gains of total pressure ratio are redesigned to maximize the adiabatic efficiency with the constraints of mass flow rate and the corresponding optimized total pressure ratio. The optimization results are presented in detail; and the effects of blade profile modification on adiabatic efficiency, total pressure ratio and shock/tip-leakage interaction are analyzed.

II. Rotor 67 Flow Validations

NASA Rotor 67 is a transonic axial-flow compressor blade in the first-stage rotor of a two-stage fan. The rotor has 22 blades and an aspect ratio of 1.56. The design total pressure ratio is 1.63 at a mass flow rate of 33.25 kg/s. The rotational speed is 16.043 rpm. The tip speed is 429 m/s with a relative Mach number of 1.38 at the inlet. The Reynolds number based on the axial chord at the hub is 1.797×10^6. Rotor 67 was developed in the 1970s and was then experimentally investigated. Strazisar et al.[20] presented the performance of Rotor 67 in detail and thus provided a data base, with which the computational results presented in the present study are compared and verified.

Leakage flow contributes a considerable part to the total flow loss of rotors. Due to its significant influence on the aerodynamic performance, many reports on numerical simulation of tip leakage flow have been published.[21–26] The spanwise distance of tip clearance of Rotor 67 is approximately $1.0mm$. The design optimization presented in the study includes the effects of tip clearance. The flow through Rotor 67 is transonic near the blade tip and the shock/tip-leakage interaction has detrimental effects on the rotor performance, such as aerodynamic losses, blockage and instabilities. Hereby, the present research concentrates on (1) how to improve the performance as required by using the viscous adjoint method; and (2) how the blade profile modification influences the shock/tip-leakage interaction.

In the present study, the Spalart-Allmaras one-equation turbulence model[27] is used to simulate the turbulent flow. The governing flow equation with a source term is given as

$$\frac{\partial \mathbf{w}}{\partial t} + \frac{\partial(\mathbf{f}_j - \hat{u}_j \mathbf{w})}{\partial x_j} = \frac{\partial \mathbf{f}_{v,j}}{\partial x_j} + \mathbf{S}, \quad j = 1, 2, 3 \tag{3}$$

where $\hat{u}_j$ and $\mathbf{S}$ are grid velocity components and the source term, respectively; and

$$\begin{aligned} &\hat{u}_1 = 0, \quad \hat{u}_2 = -\Omega x_3, \quad \hat{u}_3 = \Omega x_2 \\ &\mathbf{S} = \{0,\ 0,\ \rho u_3 \Omega,\ -\rho u_2 \Omega,\ 0\}^T \end{aligned} \tag{4}$$

Chima[25] and Kirtley et al.[28] suggested that a simple periodicity clearance model is adequate for capturing the effect of tip leakage flow. Such a model is used in the present study. An H-grid containing 120, 48 and 44 cells in the axial, pitchwise and spanwise directions, respectively, is used for flow calculations. Only 4 cells are used in the clearance gap. Although 4 cells might not be enough to accurately capture the detailed leakage flow within the clearance gap, the model is sufficient for providing information on the effect of the tip leakage flow on the main passage flow and also on the shock/tip-leakage interaction.

Figure 1 presents the overall performance of Rotor 67. The flow calculations are performed with different back pressure to obtain the total pressure ratio π and adiabatic efficiency η. In this picture, the mass flow rates of the CFD and experiment are normalized by their corresponding choked values. The total pressure ratio and adiabatic efficiency obtained from CFD agree with those of experiment.

Figure 2 presents the computed spanwise distributions of total pressure ratio π, total temperature ratio θ and flow turning β near peak efficiency. The results are compared with those of experiment. In order to illustrate the influence of clearance gap on the aerodynamic performance, flow calculation without gap is also performed with the same back pressure. In this picture, with the clearance gap the flow turning

has a significant increment, while the total pressure ratio is significantly decreased near the casing. The clearance gap reduces the capability for the blade to impart work to the flow near the blade tip. On the other hand, the shock/tip-leakage interaction leads to an axial momentum deficit and consequently the flow turning increases. Van Zante et al.[22] and Dunham et al.[29] confirmed the increase of total temperature in the gap through numerical simulation and experimental measurement and suggested that the total temperature excess was attributed to the increased flow turning of the leakage flow. The computed spanwise distributions with clearance gap agree well with experiment.

III. Descriptions of Multi-Objective Optimization

In the present study, multi-objective optimization is completed by two steps, which are referenced below as design initialization and Pareto front determination, respectively. The design initialization attempts to maximize the total pressure ratio with the constraint of mass flow rate. The cost function is defined as

$$I = \frac{1}{\pi} + \Lambda|\sigma - 1| \tag{5}$$

with the subject

$$1 \leq \hat{\pi} = \frac{\pi}{\pi_0} \leq \hat{\pi}_{max} \tag{6}$$

where $\hat{\pi}$ is the ratio of the total pressure ratio of the optimized blade π to that of the reference blade π_0; $\hat{\pi}_{max}$ is the upper limit of the total pressure ratio. Through design initialization, a set of initialized blades with different gains of total pressure ratio can be obtained and the upper limit $\hat{\pi}_{max}$ can be approximately determined to avoid stall in the design.

The single-objective optimization for determining the Pareto front, starting from the initialized blades, concentrates on maximizing the adiabatic efficiency. High efficiency means low flow loss. Denton[30] suggested that all kinds of flow losses can be measured by entropy production. Consequently the entropy production per unit mass flow rate is selected as the cost function. Constraints on mass flow rate and total pressure ratio are enforced by incorporating penalty functions in the cost function. The cost function with constraints is given as

$$I = s_{gen} + \Lambda_1|\sigma - 1| + \Lambda_2|\hat{\pi} - 1| \tag{7}$$

where s_{gen} denotes the entropy production per unit mass flow rate with the definition

$$s_{gen} = \frac{\int_B n_j \rho u_j \Delta s dB}{\int_B n_j \rho u_j dB} \tag{8}$$

Minimization of the cost function described above attempts to obtain an optimized blade profile that maximizes the adiabatic efficiency for the same total pressure ratio and mass flow rate.

The profiles of nine blade sections along span are selected to be redesigned in the present study. Hicks-Henne shape functions[11] are introduced to perturb the reference blade profile and 16 shape functions are uniformly distributed each on the pressure and the suction surfaces at each of the selected blade sections.

IV. The Adjoint Method

The implementation of the adjoint method was described previously.[9,11] It is briefly summarized herein.

Let $\mathbf{R}(\mathbf{w}, \mathcal{F}) = 0$ be the steady Reynolds-Averaged Navier-Stokes (RANS) equations, where the dependence on the blade geometry through boundary conditions are explicitly specified. The variation of cost function δI and the variation of governing flow equation $\delta\mathbf{R}$ consist of two terms, one due to the variation of flow field $\delta\mathbf{w}$ and the other due to the modification of boundaries $\delta\mathcal{F}$. By introducing a set of adjoint variables and regarding the variation of governing flow equation as a constraint $\delta\mathbf{R} = 0$, the variation of cost function can be written as

$$\delta I = \{\frac{\partial I}{\partial \mathbf{w}} - \Psi^T \frac{\partial \mathbf{R}}{\partial \mathbf{w}}\}\delta\mathbf{w} + \{\frac{\partial I}{\partial \mathcal{F}} - \Psi^T \frac{\partial \mathbf{R}}{\partial \mathcal{F}}\}\delta\mathcal{F} \tag{9}$$

The key of the adjoint method is to eliminate the contribution of $\delta\mathbf{w}$ to δI through the solution of the adjoint equation in order to calculate the gradient with high efficiency. From Eq. (9) the adjoint equation

and the gradient $\mathbf{G}$ are

$$\frac{\partial I}{\partial \mathbf{w}} - \Psi^T \frac{\partial \mathbf{R}}{\partial \mathbf{w}} = 0, \quad \mathbf{G} = \frac{\partial I}{\partial \mathcal{F}} - \Psi^T \frac{\partial \mathbf{R}}{\partial \mathcal{F}} \tag{10}$$

Once the flow variables $\mathbf{w}$ and the adjoint variables Ψ are obtained through solving the governing flow equation and the corresponding adjoint equation each once, the gradient can then be calculated after obtaining some additional grid deformation information using a direct finite-difference method, which costs little computer time.

Source terms due to rotation must be included in the governing flow equations and appropriate boundary conditions in terms of the relative velocity must be imposed for the flow in a rotor blade row. The source term $\mathbf{S}$ in the governing flow equation contributes an additional adjoint source term; and meanwhile, the corresponding adjoint boundary conditions are redetermined accordingly. The viscous adjoint equation corresponding to Eq. (3) can be given as

$$\mathbf{A}_{s,j}^T \frac{\partial \Psi}{\partial x_j} + \mathbf{B}_s^T \Psi + \frac{1}{J}[\mathbf{M}^{-1}]^T \mathbf{Y} = 0 \tag{11}$$

where $\frac{1}{J}[\mathbf{M}^{-1}]^T \mathbf{Y}$ is the viscous adjoint operator as presented in the reference;[9] $\mathbf{A}_{s,j}$ and $\mathbf{B}_s$ are the Jacobian matrices and the source matrix with the definitions

$$\mathbf{A}_{s,j} = \mathbf{A}_j - \hat{u}_j \mathbf{I}_e, \quad \mathbf{B}_s = \frac{\partial \mathbf{S}}{\partial \mathbf{w}} \tag{12}$$

where $\mathbf{I}_e$ denotes the unit matrix.

The determination of the wall boundary conditions of the adjoint equation is quite similar to that presented in the previous publications. The adjoint variables on inviscid wall satisfy

$$\sum_{j=1}^{3} n_j(\psi_{j+1} + \hat{u}_j \psi_5) = 0 \tag{13}$$

while on adiabatic wall, the viscous boundary conditions of the adjoint equation are given as

$$\frac{\partial \psi_5}{\partial n} = 0, \quad \psi_{j+1} + \hat{u}_j \psi_5 = 0, j = 1, 2, 3 \tag{14}$$

Defining $\psi_j + \hat{u}_j \psi_5$ as the relative adjoint variables, it is known from Eq. (13) and Eq. (14) that the relative adjoint variables satisfy the same wall boundary conditions as those that the absolute adjoint variables satisfy in the case of a stator blade row described in the Reference.[9]

On the inlet and outlet boundaries the viscous effects can usually be neglected. For a particular case that the normal direction of the inlet and outlet boundary planes parallel with the axial direction, i.e., $n_2 = 0,\ n_3 = 0$, the determination of the inlet and outlet boundary conditions depends on only the Jacobian matrix $\mathbf{A}_{s,1}$. Since $\mathbf{A}_{s,1} = \mathbf{A}_1$ as shown by Eq. (12), it can be concluded that with a given cost function, the inlet and outlet boundary conditions of the adjoint equation are the same for inviscid and viscous design optimizations of both stator and rotor blades.

V. Results and Discussion

Before the redesign, the accuracy of the gradients obtained by the adjoint method is verified by comparing with those obtained by the finite-difference method (FDM). Figure 3 shows the gradients on 50% blade span at the first design cycle with the cost function defined as the entropy production per unit mass flow rate. The FDM gradients calculated by using different step sizes of perturbation are compared with those obtained by the adjoint method. The accuracy is acceptable.

A. Design Initialization

Design initialization concentrates on maximizing the total pressure ratio. The coefficient of the penalty function as shown in Eq. (5) is $\Lambda = 0.4$.

Figure 4 presents the variations of total pressure ratio and mass flow rate for a set of initialized blades compared with those of the reference blade. These blades are named from *Blade_1* to *Blade_10* in turn;

and *Blade*_1 is the original blade of Rotor 67. The mass flow rate is strictly enforced for all the initialized blades with the maximum discrepancy not exceeding 0.05%. Compared with *Blade*_1, the increment of total pressure ratio increases from about 1.4% of *Blade*_2 to about 10% of *Blade*_10.

Figure 5 presents the overall performance of *Blade*_1, *Blade*_3, *Blade*_6 and *Blade*_8. Blade profile modification contributes significant increment of total pressure ratio and significant decrement of adiabatic efficiency to the initialized blades over the full operating range, compared with those of the reference blade. The overall performance of the initialized blades with gains of total pressure ratio severely departs away from the reference blade. Although the present steady-state CFD approaches cannot accurately capture the true stall, the magnitude of the decrement of either mass flow rate or adiabatic efficiency near stall is usually regarded as one of the means to predict stall. Besides, the steady flow computation near stall usually converges slowly. In this figure, the mass flow rate of *Blade*_8 performs larger decline rate than other optimized blades as back pressure increases, even significantly decreases at the operating condition close to peak efficiency. Hereby an upper limit of about 8% for the total pressure ratio increment is given in the present study. The initialized blades from *Blade*_1 to *Blade*_7 are selected to be redesigned to determine the Pareto front.

B. Pareto Front Determination

The single-objective design optimization seeks to find the converged blade profiles for the multi-objective design optimization starting from the initialized blades. Nemec et al.[18] performed the multi-objective optimization of aerodynamic shape for an airfoil by using the adjoint method; and the Pareto front was obtained following an proposed convergence criterion that the L_2 norm of the gradient less than 0.01. In the present study the single-objective optimization maximizing adiabatic efficiency with the constraints of mass flow rate and total pressure ratio can be performed with another convergence criterion

$$|\frac{s_{gen,i+1}}{s_{gen,i}} - 1| \leq \delta_s \tag{15}$$

where $s_{gen,i}$ and $s_{gen,i+1}$ are the entropy production of the adjacent redesigned profiles satisfying

$$|\sigma - 1| \leq \delta_m, \quad |\hat{\pi} - 1| \leq \delta_\pi \tag{16}$$

In the present study, $\delta_s = 0.5\%$, $\delta_m = 0.05\%$, $\delta_\pi = 0.5\%$.

Figure 6 presents the Pareto front of the multi-objective design optimization. In this picture, due to the lower limit of total pressure ratio as presented in Eq. (6), the adiabatic efficiency significantly increases without loss in total pressure ratio for all the optimized blades. As total pressure ratio increases, the adiabatic efficiency decreases. Supposing the total pressure ratio is allowed to be lower than that of Rotor 67 blade, more gains of adiabatic efficiency can be achieved.

Figure 7 presents the entropy production per unit mass flow rate versus design cycles for three optimized blades, where the entropy production is normalized by the corresponding reference value. *Opt_B*1, *Opt_B*3 and *Opt_B*6 denote the optimized blades of *Blade*_1, *Blade*_3 and *Blade*_6, respectively. Within less than 150 design cycles, the entropy production approaches convergence.

In order to investigate the influence of blade profile modification on the performance improvement, the flow solutions of six different blades are presented and compared in detail. Table 1 gives the flow solutions of both the initialized and optimized blades. The mass flow rate of each optimized blade maintains almost the same as that of the corresponding initialized blade. The entropy production is normalized by that of *Blade*_1. As the total pressure ratio increases through design initialization with the constraint of mass flow rate, the shock wave appears to be stronger resulting in more flow loss along with increased entropy production and decreased adiabatic efficiency. Meanwhile, the flow turning increases due to the improved working capability. Through blade optimization, the adiabatic efficiency of each optimized blade is increased with strictly enforced mass flow rate and total pressure ratio. Compared with that of the corresponding initialized blade, the flow turning of each optimized blade is decreased.

Figure 8 and figure 9 present the pressure contours on blade surface. Compared with the reference blade *Blade*_1, design initialization strengthens the shock on the outer span, which contributes to the increase of downstream total pressure ratio and the decrease of adiabatic efficiency. Besides, as total pressure ratio increases, the shock perpendicular to the casing moves upward and locates closely to the leading edge on the pressure surface, which can also be visualized in figure 10. Such changes of shock pattern significantly

influence the aerodynamic performance, stall margin, compressor stability, etc. Through blade optimization, the shock of Opt_B1 and Opt_B6 moves downward and be significantly weakened on the outer span compared with that of the initialized blades. Hereby the total pressure ratio is decreased and the adiabatic efficiency is increased for the optimized blades. Besides, the low-pressure regions on the pressure surface of the optimized blades move toward the hub, resulting in higher downstream total pressure ratio on the inner span to maintain the overall total pressure ratio at the outlet.

Figure 10 presents the pressure distributions at two different span locations. At 25% blade span, the pressure increases on almost the whole pressure surface and a strong shock appears on the suction surface of $Blade\_6$. Through blade optimization, the shock is significantly weakened. However, on the rear portion of the optimized blades, the pressure distributions are almost the duplicates of those of the initialized blades. Such optimized pressure distributions favor increasing both total pressure ratio and adiabatic efficiency. At 95% blade span, the shock of the optimized blades moves downward and is significantly weakened, which contributes to the decrease of total pressure ratio and the increase of adiabatic efficiency. Besides, there exists an evident double-shock system on the pressure surface of the optimized blades, with the first wave more inclined upstream than the single one. The decreased loading at 95% blade span of the optimized blades contributes a decrement to flow turning. Such variations of total pressure ratio, adiabatic efficiency and flow turning are also visualized in figure 11.

In figure 11, the total pressure ratio of the optimized blades increases on the inner blade span and decreases on the outer span, compared with those of the initialized blades. The optimized flow turning keeps almost the same as that of the corresponding initialized blade. However, it decreases from 80% blade span to the blade tip. The adiabatic efficiency of the optimized blades is increased along the whole blade span due to the weakened shock.

Figure 12 presents the overall performance of the initialized and optimized blades. Compared with those of the initialized blades, the total pressure ratio of the optimized blades decreases around the 98% normalized mass flow rate and beyond, while increases below 98% normalized mass flow rate. However, the adiabatic efficiency increases over the whole operating range.

Experiment[20] suggests that Rotor 67 approaches stall at about 93% normalized mass flow rate. The true stall cannot be captured in the present study. Reasons includes (1) the steady-state flow model might not be able to simulate the high unsteady stall flow and consequently cannot capture the real stall phenomena; and (2) the numerical simulation of leakage flow is still an open issue and different turbulence models may support quite different results as shown by Biollo and Benini.[26] Whether the multi-objective design optimization offers a wider stall margin cannot be confirmed by the present steady-state code. However, as presented in figure 12, the decrement of mass flow rate of Opt_B6 below 98% normalized mass flow rate is much less than that of $Blade\_6$, which indicates that the stall margin can be improved.

Shock/tip-leakage interaction is regarded as one of the main stall triggers in transonic compressor rotors. Suder et al.[21] and Chima[25] suggested that low relative Mach number means low dynamic head along with severe flow blockage induced by shock/tip-leakage interaction. Figure 13 presents the contours of relative Mach number on the S1 streamsurface at the blade tip near stall. As total pressure ratio increases, the leakage flow spreads out and occupies almost the whole blade pitch downstream of the shock, as shown by the contour of $Blade\_6$. Through blade optimization, the region with low relative Mach number of each optimized blade is significantly reduced, compared with that of the corresponding initialized blade. However, compared with the reference blade $Blade\_1$, the region with low relative Mach number is still increased for Opt_B6. The results confirm that the rotor blade with rather high total pressure ratio inevitably approach stall at lower back pressure and the prediction of upper limit of total pressure ratio through design initialization is necessary in the adjoint-based multi-objective design optimization.

VI. Conclusion

A continuous adjoint equation method corresponding to the RANS equations is formulated and demonstrated for the aerodynamic design optimization of a transonic compressor rotor blade. The multi-objective design optimization maximizing both the total pressure ratio and adiabatic efficiency is studied.

The blade geometry of NASA Rotor 67 is redesigned by using the adjoint method. The multi-objective design optimization is completed by two steps, design initialization and Pareto front determination. The design initialization maximizing total pressure ratio alone supports a set of initialized blades and an approximate upper limit of total pressure ratio, which is verified to be necessary in the present multi-objective design

optimization. A series of single-objective optimizations starting from the initialized blades are successfully performed to maximize the adiabatic efficiency with the constraints of mass flow rate and total pressure ratio. A limited number of Pareto solutions are obtained at the design convergence and thus the Pareto front is determined. The effects of blade profile modification on aerodynamic performance improvement are presented. The results demonstrate that the optimization can significantly weaken the shock in the blade passage. Examination of tip-leakage flow also shows reduced/increased shock/tip-leakage interaction at the operating condition near stall, which indicates potential extension/reduction of stall margin.

Acknowledgments

The first author would like to thank the National Natural Science Foundation of China (Grant No. 51206003) and the National Science Foundation for Post-doctoral Scientists of China (Grant No. 2012M510267) for supporting the research work.

References

[1]Oyama, E. A., Liou, M. S., and Obayashi, S., "Transonic Axial-Flow Blade Shape Optimization: Evolutionary Algorithm/Three-Dimensional Navier-Stokes Solver," *Journal of Propulsion and Power*, Vol. 20, No. 4, 2004, pp. 612-619

[2]Samad, A., Kim, K. Y., Goel, T., Haftka, R. T., and Shyy, W., "Multiple Surrogate Modeling for Axial Compressor Blade Shape Optimization," *Journal of Propulsion and Power*, Vol. 24, No. 2, 2008, pp. 301-310

[3]Benini, E., "Three-Dimensional Multi-Objective Design Optimization of a Transonic Compressor Rotor," *Journal of Propulsion and Power*, Vol. 20, No. 3, 2004, pp. 559-565

[4]Lian, Y., and Liou, M. S., "Multi-Objective Optimization of Transonic Compressor Blade Using Evolutionary Algorithm," *Journal of Propulsion and Power*, Vol. 21, No. 6, 2005, pp. 979-987

[5]Jameson, A., "Aerodynamic Design via Control Theory," *Journal of Scientific Computing*, Vol. 3, No. 3, 1988, pp. 233-260

[6]Jameson, A., "Aerodynamic Shape Optimization Using the Adjoint Method," Lectures at the von-Karman Institute, February, 2003

[7]Yang, S., Wu, H., Liu, F., and Tsai, H. M., "Aerodynamic Design of Cascades by Using an Adjoint Equation Method," AIAA Paper 2003-1068, January, 2003

[8]Wu, H., Liu, F., and Tsai, H. M., "Aerodynamic Design of Turbine Blades Using an Adjoint Equation Method," AIAA Paper 2005-1006, January, 2005

[9]Luo, J., Xiong, J., Liu, F., and McBean, I., "Secondary Flow Reduction by Blade Redesign and Endwall Contouring Using an Adjoint Optimization Method," ASME Paper GT2010-22061, June, 2010

[10]Luo, J., Liu, F., and McBean, I., "Optimization of Endwall Contours of a Turbine Blade Row Using an Adjoint Method," ASME Paper GT2011-46163, June, 2011

[11]Luo, J., Xiong, J., Liu, F., and McBean, I., "Three-Dimensional Aerodynamic Design Optimization of a Turbine Blade by Using an Adjoint Method," *Journal of Turbomachinery*, Vol. 133, No. 1, 2011

[12]Luo, J., Zhou, C., and Liu, F., "Multi-Point Design Optimization of a Transonic Compressor Blade by Using an Adjoint Method," ASME Paper GT2013-95155, June, 2013

[13]Wang, D., and He, L., "Adjoint Aerodynamic Design Optimization for Blades in Multi-Stage Turbomachines: Part I-Methodology and Verification," *Journal of Turbomachinery*, Vol. 132, No. 2, 2010

[14]Wang, D., He, L., Wells, R., and Chen, T., "Adjoint Aerodynamic Design Optimization for Blades in Multi-Stage Turbomachines: Part II-Validation and Application," *Journal of Turbomachinery*, Vol. 132, No. 2, 2010

[15]Walther, B., and Nadarajah, S., "Constrained Adjoint-Based Aerodynamic Shape Optimization of a Single-Stage Transonic Compressor," *Journal of Turbomachinery*, Vol. 135, No. 2, 2013

[16]Sevastyanov, V., "Gradient-Based Multi-Objective Optimization Technology," AIAA Paper 2010-9092, September, 2010

[17]Shankaran, S., and Barr, B., "Efficient Gradient-Based Algorithm for the Construction of Pareto Front," ASME Paper GT2011-45069, June, 2011

[18]Nemec, M., Zingg, D. W., and Pulliam, T. H., "Multipoint and Multi-Objective Aerodynamic Shape Optimization," *AIAA Journal*, Vol. 42, No. 6, 2004, pp. 1057-1065

[19]Kee Lee, C. J., Furuya, W., Tanaka, M., and Takano, N., "Adjoint Variable Method for Multi-Objective Sizing and Shape Optimization," *Journal of Computational Science and Technology*, Vol. 3, No. 1, 2009, pp. 275-286

[20]Strazisar, A. J., Wood, J. R., Hathaway, M. D., and Suder, K. L., "Laser Anemometer Measurements in a Transonic Axial-Flow Fan Rotor," NASA TP 2879, November, 1989

[21]Suder, K. L., and Celestina, M. L., "Experimental and Computational Investigation of the Tip Clearance Flow in a Transonic Axial Compressor Rotor," *Journal of Turbomachinery*, Vol. 118, No. 2, 1996, pp. 218-229

[22]Van Zante, D. E., Strazisar, A. J., Wood, J. R., Hathaway, M. D., and Okiishi, T. H., "Recommendations for Achieving Accurate Numerical Simulationof Tip Clearance Flows in Transonic Compressor Rotors," NASA/TM–2000-210347, September, 2000

[23]Arnone, A., "Viscous Analysis of Three-Dimensional Rotor Flows Using a Multigrid Method," NASA/TM–1993-106266, July, 1993

[24]Puterbaugh, S. L., and Brendel, M., "Tip Clearance Flow-Shock Interaction in a Transonic Compressor Rotor," *Journal of Propulsion and Power*, Vol. 13, No. 1, 1997, pp. 24-30

[25]Chima, R. V., "Calculation of Tip Clearance Effects in a Transonic Compressor Rotor," *Journal of Turbomachinery*, Vol. 120, No. 1, 1998, pp. 131-140

[26]Biollo, R., and Benini, E., "Shock/Boundary-Layer/Tip-Clearance Interaction in a Transonic Rotor Blade," *Journal of Propulsion and Power*, Vol. 25, No. 3, 2009, pp. 668-677

[27]Spalart, P. R., and Allmaras, S. R., "A One-Equation Turbulence Model for Aerodynamic Flows," AIAA Paper 1992-0439, January, 1992

[28]Kirtley, K. R., Beach, T. A., and Adamczyk, J. J., "Numerical Analysis of Secondary Flow in a Two-Stage Turbine," AIAA Paper 1990-2356, July, 1990

[29]Dunham, J., and Meauze, G., "An AGRAD Working Group Study of 3D Navier-Stokes Codes Applied to Single Turbomachinery Blade Rows," ASME Paper 98-GT-50, June, 1998

[30]Denton, J. D., "Loss Mechanisms in Turbomachines," *Journal of Turbomachinery*, Vol. 115, No. 4, 1993, pp. 621-656

Table 1. Performance of both reference and all of the optimized blades

Blades	s_{gen}	$\dot{m}$(kg/s)	π	η(%)	β(deg)
Blade_1	1.000	34.59	1.627	92.09	-38.85
Blade_3	1.140	34.59	1.675	91.48	-41.09
Blade_6	1.261	34.57	1.724	91.06	-43.19
Opt_B1	0.906	34.59	1.628	92.81	-38.81
Opt_B3	0.967	34.60	1.672	92.55	-40.75
Opt_B6	0.988	34.59	1.716	92.46	-42.58

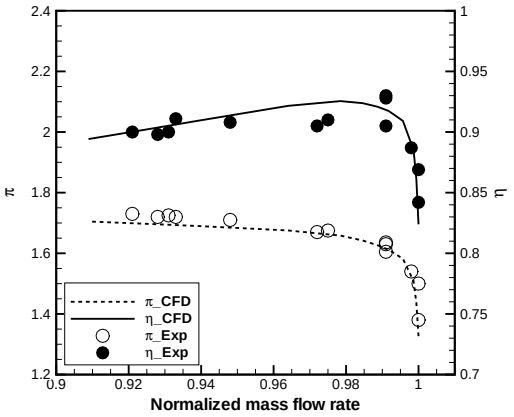

Figure 1. Comparisons of operating performance

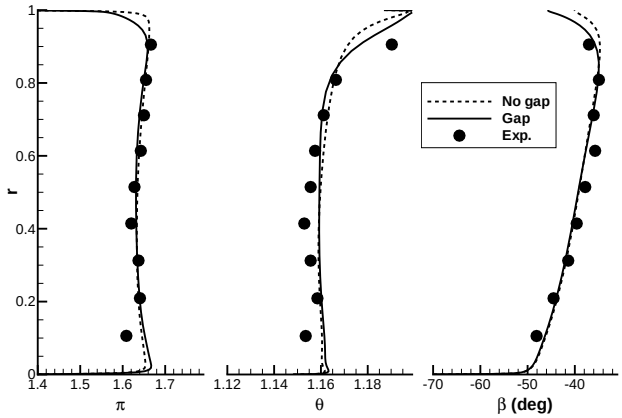

Figure 2. Spanwise distributions of total pressure ratio, total temperature ratio and flow turning

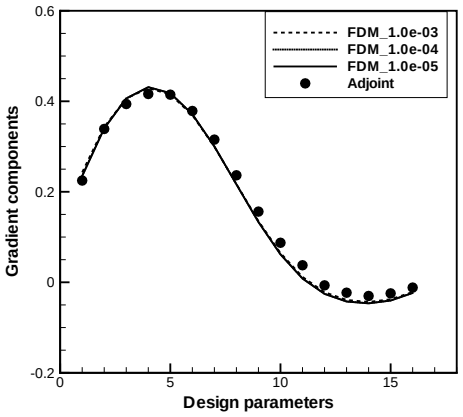

Figure 3. Comparisons of gradients

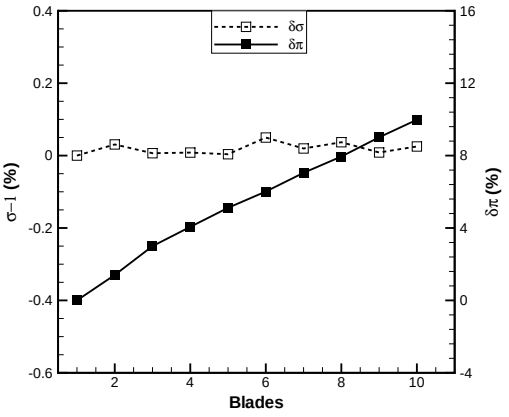

Figure 4. Mass flow rate and total pressure ratio for different optimized blades

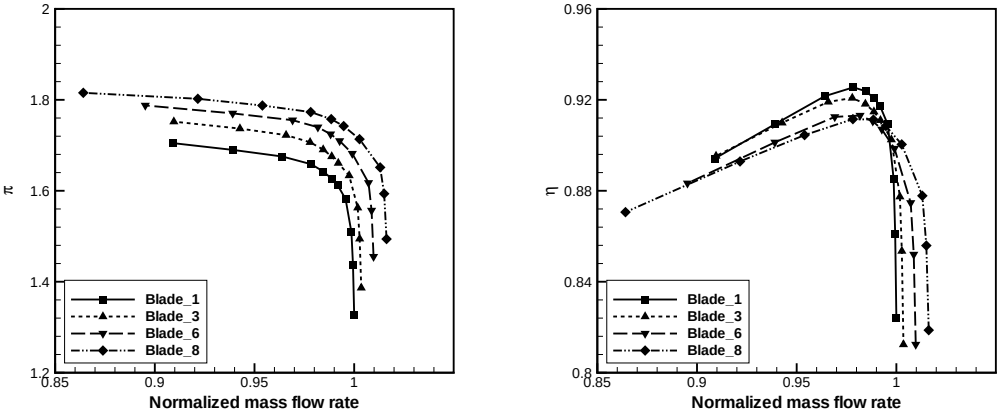

Figure 5. Operating characteristics for reference and optimized blades

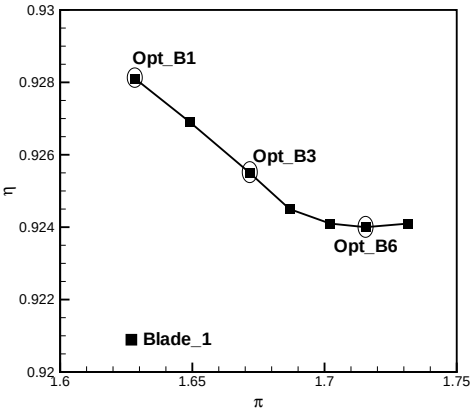

Figure 6. Pareto front

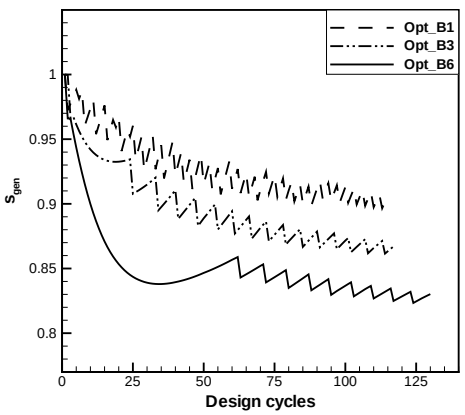

Figure 7. Cost function versus design cycles

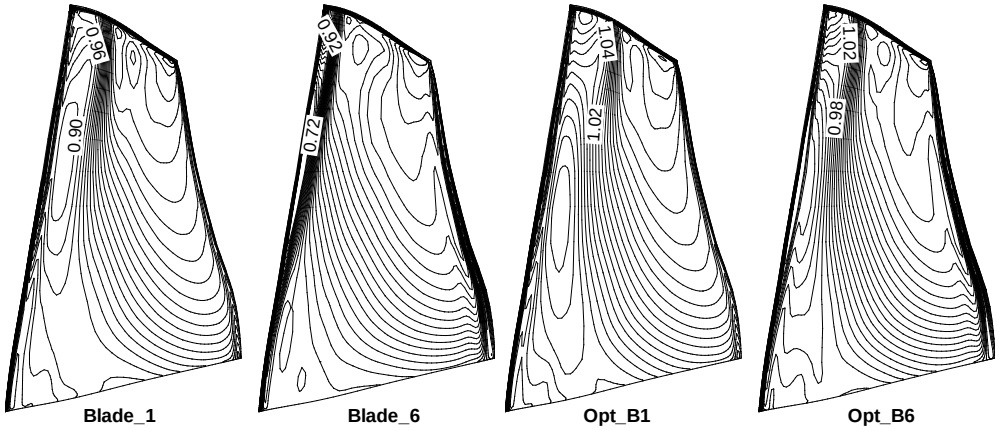

Figure 8. Pressure contours on blade pressure surface

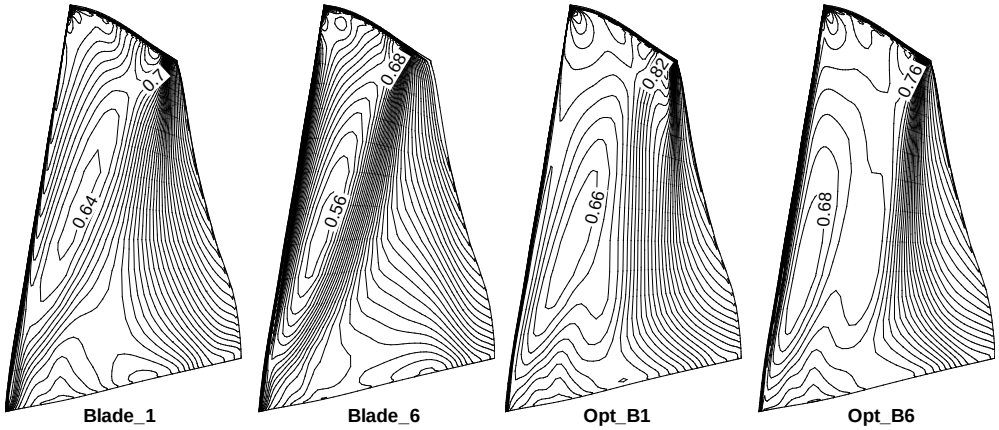

Figure 9. Pressure contours on blade suction surface

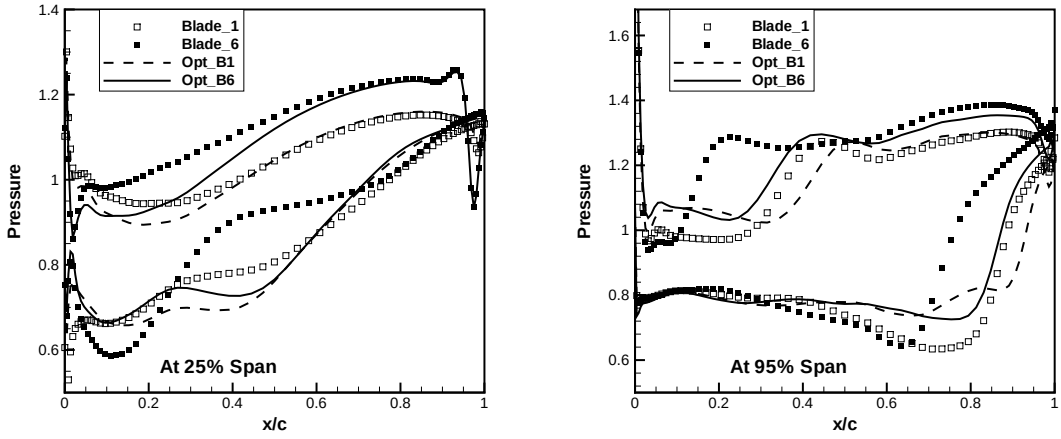

Figure 10. Pressure distributions at different span locations

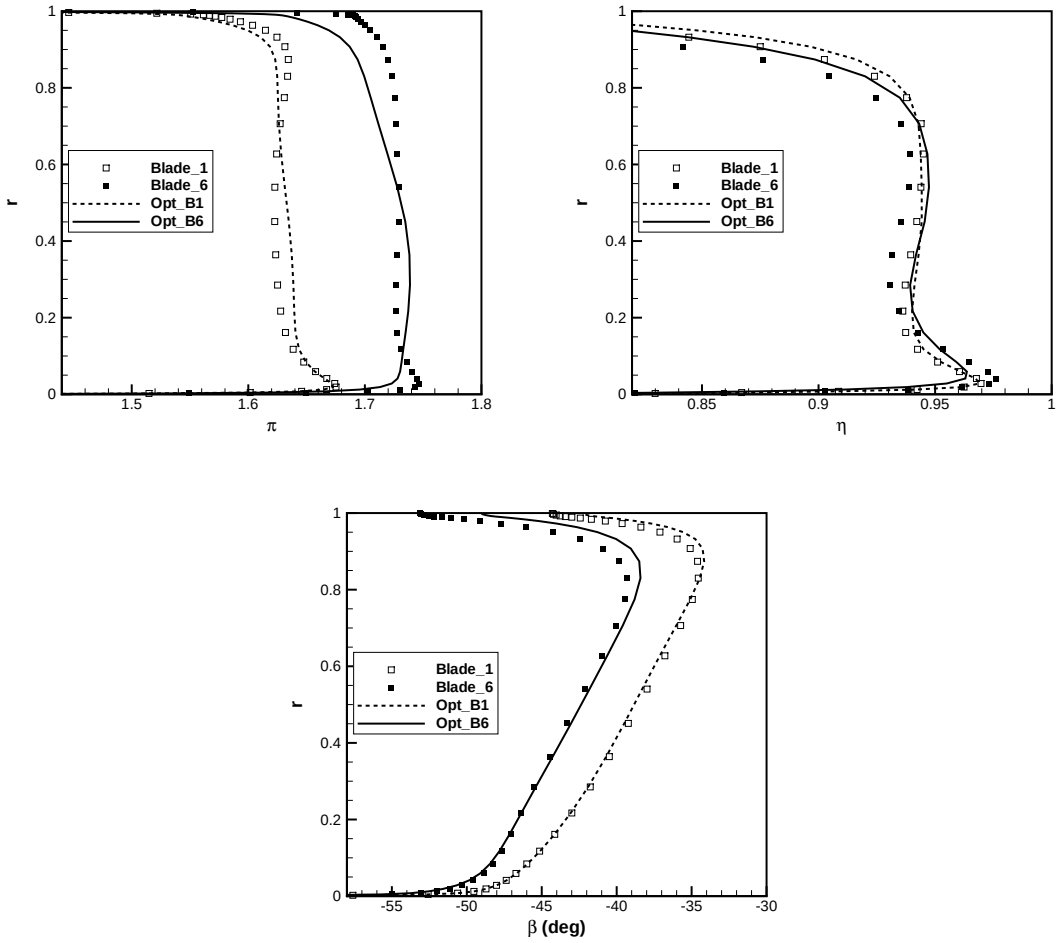

Figure 11. Spanwise distributions of: ***total pressure ratio, adiabatic efficiency and flow turning***

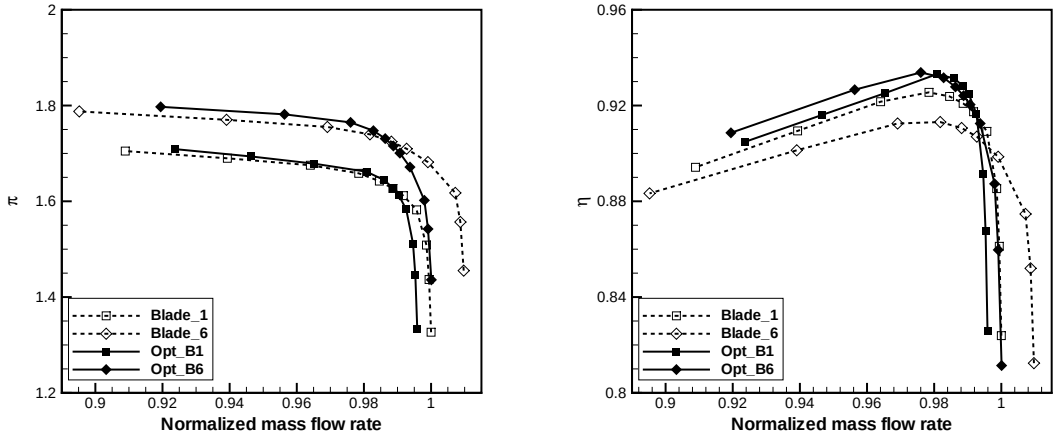

Figure 12. Operating characteristics for reference and optimized blades

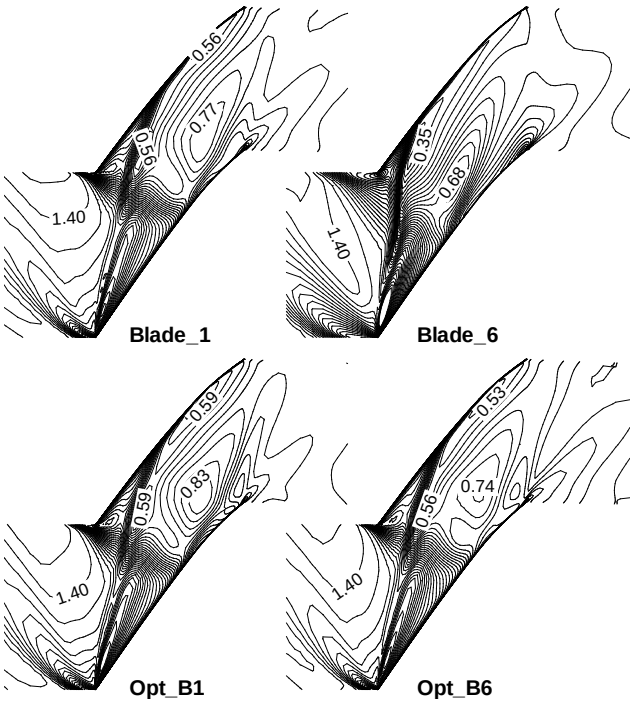

Figure 13. Contours of relative Mach number on a blade-to-blade streamsurface at the blade tip